

Opposite seasonality of the aerosol optical depth and the surface particulate matter concentration over the north China Plain



Wenjun Qu^{a,*}, Jun Wang^b, Xiaoye Zhang^c, Lifang Sheng^a, Wencai Wang^a

^a Physical Oceanography Laboratory, Key Laboratory of Ocean-Atmosphere Interaction and Climate in Universities of Shandong, Ocean University of China, Qingdao 266100, China

^b Department of Earth and Atmospheric Sciences, University of Nebraska-Lincoln, Lincoln, NE 68588-0340, USA

^c Chinese Academy of Meteorological Sciences, China Meteorological Administration, Beijing 100081, China

HIGHLIGHTS

- The AOD seasonality is distinct over NCP (maximum in June and minimum in December).
- BLH, RH collaborate with PM concentration can well explain monthly AOD variation.
- June AOD increase over NCP relates to prevailing of the East Asia summer monsoon.

ARTICLE INFO

Article history:

Received 13 July 2015

Received in revised form

26 November 2015

Accepted 28 November 2015

Available online 8 December 2015

Keywords:

Aerosol optical depth

Seasonality

Boundary layer height

North China Plain

ABSTRACT

Great difference exists in the aerosol optical depth (AOD) between summer and winter over the North China Plain (NCP). Monthly mean AOD at 550 nm derived from the MODIS (MODerate Resolution Imaging Spectroradiometer) products during 2000–2014 over the area of 30–40° N and 110–125° E exhibits an annual maximum in June (0.855 ± 0.130) and a minimum in December (0.381 ± 0.032). This seasonality of AOD is in the opposite phase with the surface particulate matter (PM) concentration (higher in winter and lower in summer). The possible causes for the higher AOD in June (compared with December) include (a) a higher boundary layer height (BLH) that results in more efficient transport and mixing of aerosol particles to a higher altitude (corresponding to a lower particle concentration near surface) as revealed by the Cloud-Aerosol Lidar and Infrared Pathfinder Satellite Observations profile, (b) a higher relative humidity (RH) due to the inshore monsoon circulation that leads to enhancement of aerosol extinction, (c) emission from the regional open stalk burning in the summer harvest season (as seen from MODIS fire products), and (d) the typical eastward open topographical basin over NCP. Under the assumption that the aerosol and water vapor are well mixed within the boundary layer, analysis on multi-year average shows that the differences in BLH, RH and surface PM concentration can explain up to 81% of the variance of monthly averaged AOD over NCP. A preliminary hypothesis is also suggested to interpret the shift of AOD pattern from winter to summer with an abrupt increase of AOD from May to June, as well as an increase of surface PM_{2.5} concentration over NCP during the early phase of northward progress of the East Asia summer monsoon front.

© 2015 Elsevier Ltd. All rights reserved.

1. Introduction

Satellite measurement has been applied to air quality monitoring worldwide including the North China Plain (NCP, Li et al., 2003); although a good relationship has been established

between the MODerate Resolution Imaging Spectroradiometer (MODIS) aerosol optical depth (AOD) and surface PM_{2.5} (particulate matter (PM) with diameter $\leq 2.5 \mu\text{m}$) concentration in eastern and Midwestern USA (Engel-Cox et al., 2004) and Alabama (Wang and Christopher, 2003), correlation between AOD and surface PM_{2.5} is quite poor in western USA (Engel-Cox et al., 2004). A critical review by Hoff and Christopher (2009) concluded that the derivation of surface PM_{2.5} from satellite measurement of AOD (with a precision of $\pm 20\%$) has an uncertainty of $\pm 30\%$ (or larger), AOD should

* Corresponding author. Physical Oceanography Laboratory, Ocean University of China, Qingdao 266100, China.

E-mail addresses: quwj@ouc.edu.cn, quwj@163.com (W. Qu).

combine with ground-based measurement and model to improve PM estimation from space.

Li et al. (2003) validated the MODIS aerosol products and identified three high AOD areas in eastern China (ECN). In north China, a discrepancy in the seasonal variations of AOD and surface particle concentration has been identified, which was partly attributed to the variation of atmospheric mixing layer height (Xia et al., 2006). Wang et al. (2012) reported the contrasting trends between PM₁₀ and the aerosol optical extinction in China, USA, Canada and Europe from 1992 to 2011, and emphasized contribution from the increased fraction of anthropogenic aerosol emission (mostly fine particle). Besides the vertical profile and size distribution of the aerosol, are there any other factors also contribute to the seasonal variation of AOD in north China?

While the wintertime air pollution (as well as haze and fog) is recognized as a major concern in ECN (Yang et al., 2013a; Zhao et al., 2013; Boynard et al., 2014), past studies also investigated the increasing trend of summertime air quality deterioration in the region from both the meteorology (Qu et al., 2013) and the emission (Li et al., 2010) perspectives. An overall comparatively better surface air quality in summer (than in winter) over ECN can be easily understood because of the greater boundary layer height (BLH) which is more favorable for dilution and diffusion of the pollutants as well as the more intensive precipitation which is more favorable for wet scavenging of the particle. For example, the surface fine particle concentration in Wuhan, China was found to be mainly depends on variation in the convective BLH (Kong and Yi, 2015). However, it is interesting that the better air quality and lower PM concentration near surface in summer is in contrast with the higher summertime AOD (will be discussed in section 3) over NCP (generally the area of 30–40° N and 110–125° E, Fig. 1). This study will examine the factors contributing to the higher AOD in June (compared with the lower AOD in December) over NCP.

2. Data

The data used in this study include MODIS Terra AOD products (1 × 1° grid) from March 2000 to December 2014 from Giovanni (<http://giovanni.gsfc.nasa.gov/giovanni/>) and the GOCART (Goddard Chemistry Aerosol Radiation and Transport, Mian et al., 2002) modeled CODs (column optical depth) for different aerosol components in 2000–2007 (formerly distributed by Giovanni, accessed by July 2015), as well as the AERONET AOD data at Beijing (116.381° N, 39.977° E) from March 2001 to October 2013 (http://aeronet.gsfc.nasa.gov/cgi-bin/webtool_operav2_new). The aerosol extinction coefficient at 532 nm derived from the Cloud-Aerosol Lidar and Infrared Pathfinder Satellite Observations (CALIPSO) level 3 allsky product (https://eosweb.larc.nasa.gov/project/calipso/cal_lid_l3_apro_allsky-beta-v1-30_table) is used to reflect vertical distribution of the aerosol. Relative humidity (RH) and wind (2.5 × 2.5° grid) from NCEP (United States National Centers for Environmental Prediction) reanalysis data (<http://www.esrl.noaa.gov/psd/data/gridded/data.ncep.reanalysis.html>) and BLH (0.125 × 0.125° grid) from ECMWF (European Center for Medium-Range Weather Forecasts) reanalysis data (<http://apps.ecmwf.int/datasets/>) are also used to make comparison of meteorology between summer and winter.

In addition, the available PM₁₀ (particles with diameter ≤ 10 μm) concentration in 34 major Chinese cities over NCP from 2005 to 2012 is derived from the air pollution index from the Ministry of Environment Protection of China (MEPC, <http://datacenter.mep.gov.cn/>) using the method in Qu et al. (2010). Similarly, the available PM_{2.5} concentration in 142 Chinese cities in 2014 is also derived from the air quality index from MEPC. These data are used to reflect the seasonal variation of surface PM

concentration over NCP.

Moreover, the surface visibility (Vis), wind speed and RH extracted from the Global Summary of Day (GSOD) database (<ftp://ftp.ncdc.noaa.gov/pub/data/g sod>) for 354 stations in China are used to assess impact of the northward progress of East Asia summer monsoon. Detail of these data is described in Qu et al. (2013, 2015b).

3. Contrast between AOD and surface PM seasonality over NCP

The mean MODIS Terra AOD at 550 nm over China during 2000–2014 demonstrates that the AOD seasonal contrast is most distinct over NCP; AOD in June is generally larger than 0.6 (>0.9 over most of the area, Fig. 1a) and AOD in December generally ranges from 0.36 to 0.6 over NCP (Fig. 1b, also see supplementary material 1 for the yearly comparison), which reflects the greatest seasonal difference of monthly AOD in China. NCP is also the major high AOD area in China; the AOD hotspot area over NCP is generally constrained within the NCP topographical basin (supplementary material 1), which is expected because the basin is always most densely populated with intensive anthropogenic emission, consistent with Li et al. (2003) that human activities are the main source of aerosols in ECN. In addition, the obvious interannual variation in spatial coverage of the higher AOD area over ECN (supplementary material 1) is beyond the scope of this study.

Fig. 2 shows the time series of AOD and surface PM concentration. The monthly averaged MODIS Terra AOD at 550 nm over NCP during 2000–2014 obviously illustrates an annual maximum in June (0.855 ± 0.130, Fig. 2a) and a minimum in December (0.381 ± 0.032). The AERONET monthly averaged AOD at Beijing (Fig. 2b) generally shows a synchronous variation with the MODIS AOD over NCP, and significant correlations ($R = 0.72–0.75$, $P < 0.0001$ significance, $n = 135$) exist between the monthly averaged AERONET AODs at 440 nm, 675 nm, 870 nm and 1020 nm at Beijing with the monthly averaged MODIS AOD over NCP.

Fig. 2c shows monthly surface PM₁₀ mass concentration in 34 major Chinese cities over NCP from 2005 to 2012. In discrepancy with the higher AOD in June (compared with the lower AOD in December), the surface PM₁₀ concentration in June is generally lower than that in December; similarly, the PM_{2.5} concentration varies in a same way as PM₁₀ (supplementary material 2). It must be noted here that the MODIS AOD is an ambient measurement, but the surface PM measurement is generally made by using of the Tapered Element Oscillating Microbalance analyzers (TEOMs, model 1400a, Rupprecht & Patashnick, USA) at an elevated temperature (50 °C), thus suffers loss of materials such as the semi-volatile and hygroscopic species (see detail in Qu et al., 2010). A discussion of the possible causes resulting in such contrast between the phase of monthly variation of AOD and PM will follow.

4. Possible causes of the AOD seasonality over NCP

4.1. Emission

Over ECN, the presumably intensive and continuous anthropogenic emission (of the aerosol and its precursor gases) due to house heating is believed to be an important additional source in winter. Such an intensive anthropogenic emission in winter is supported by the high wintertime black carbon and brown carbon concentration reported in Beijing during 2002–2013 (Li et al., 2015). Meanwhile, the higher mineral dust concentration in Beijing in spring (Li et al., 2015) is consistent with the more intensive springtime dust emission.

On the other hand, an inspection of global fire maps from the National Aeronautics and Space Administration earth observatory

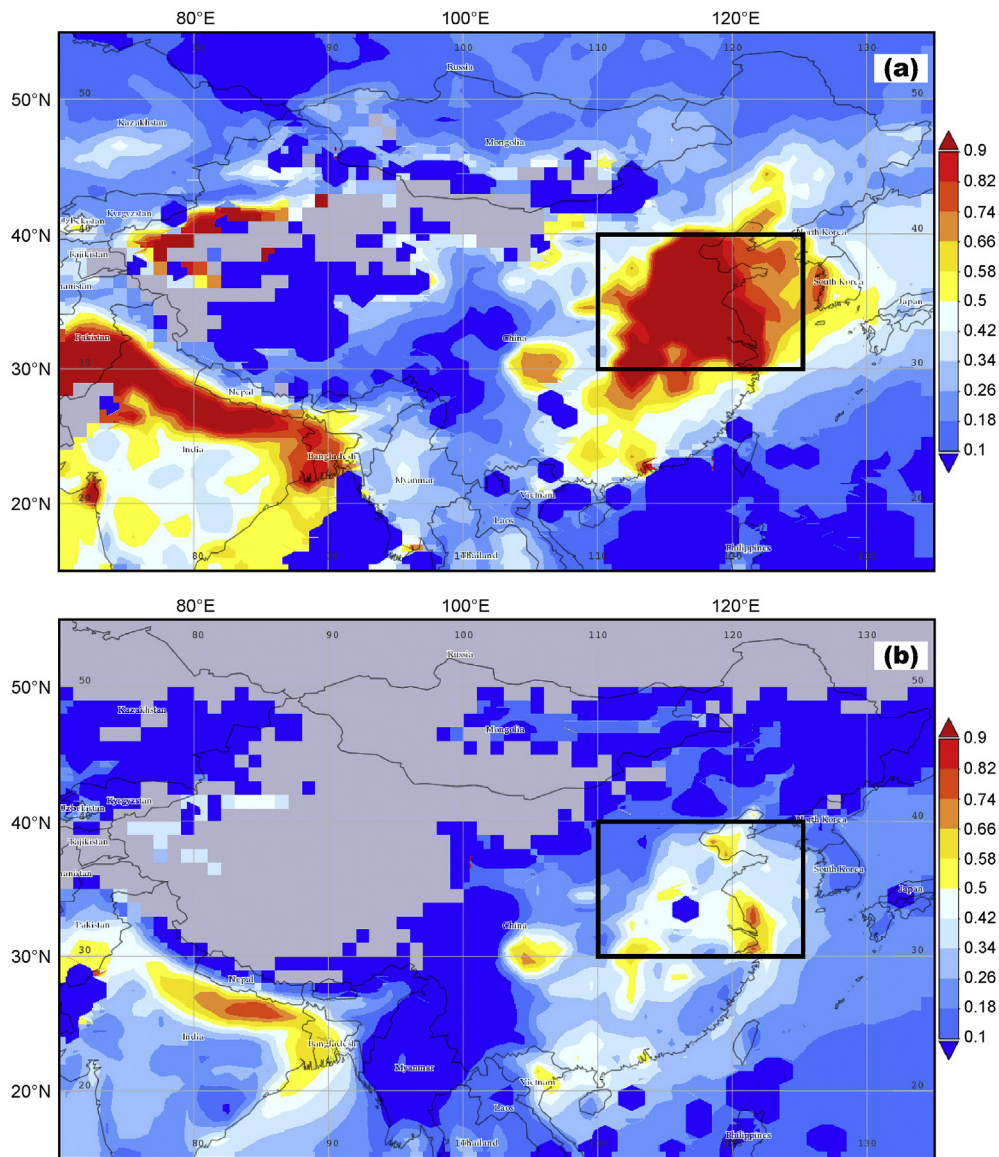


Fig. 1. The mean MODIS Terra AOD at 550 nm over China in (a) June and (b) December during 2000–2014. The AOD contrast is significant over NCP (the area of 30–40° N and 110–125° E, indicated by a black box with the North China Plain as a principal part).

system (http://www.earthobservatory.nasa.gov/GlobalMaps/view.php?d1=MOD14A1_M_FIRE#) shows clear fire points from Shandong Peninsula to the north of Yangtze River in ECN (the major NCP area) in June every year, suggesting potential additional emission sources favorable for high AOD over this area in June. Such an additional June emission is most probably associated with the regional intensive open stalk burning in the summer harvest season. Individual particle study did identify evidence of the contribution from regional agricultural biomass burning to high AOD in Beijing and north China in June 2007 (Li et al., 2010). This regional *open, out-of-order* and *uncontrolled* stalk burning is a major emission source over NCP in the summer harvest season. For example, the agricultural biomass burning has been found to be associated with the AOD peak value in June over ECN (Yang et al., 2013b). Observation of a clearly increased black carbon concentration in June (comparable with those in December, January and February) at Beijing (Li et al., 2015) also supports this point.

In addition to emission, BLH (associated with vertical distribution of the aerosol) and meteorology (including wind and RH) are

the other important factors influencing AOD and PM concentration and will be discussed next.

4.2. BLH and vertical extinction profile

Δ BLH, defined as the difference of BLH at 14:00 local time (derived from ECMWF model, see section 2) between June and December during 2000–2013, shows that BLH in June is generally greater than BLH in December by at least 350 m over the AOD hotspots area from Shandong Peninsula to the north of Yangtze River in ECN (i.e., NCP, Fig. 3a); the higher BLH could result in more efficient transport and mixing of particles to a higher altitude (layer), leading to an increase of column AOD in June (compared to December) but possibly a decrease of surface PM concentration, consistent with Kong and Yi (2015).

A comparison of the CALIPSO extinction profiles between June and December in 2014 over NCP (Fig. 3b) does illustrate a higher extinction coefficient in June at a higher altitude, especially above ~600 m where both the day and night extinction coefficients in June

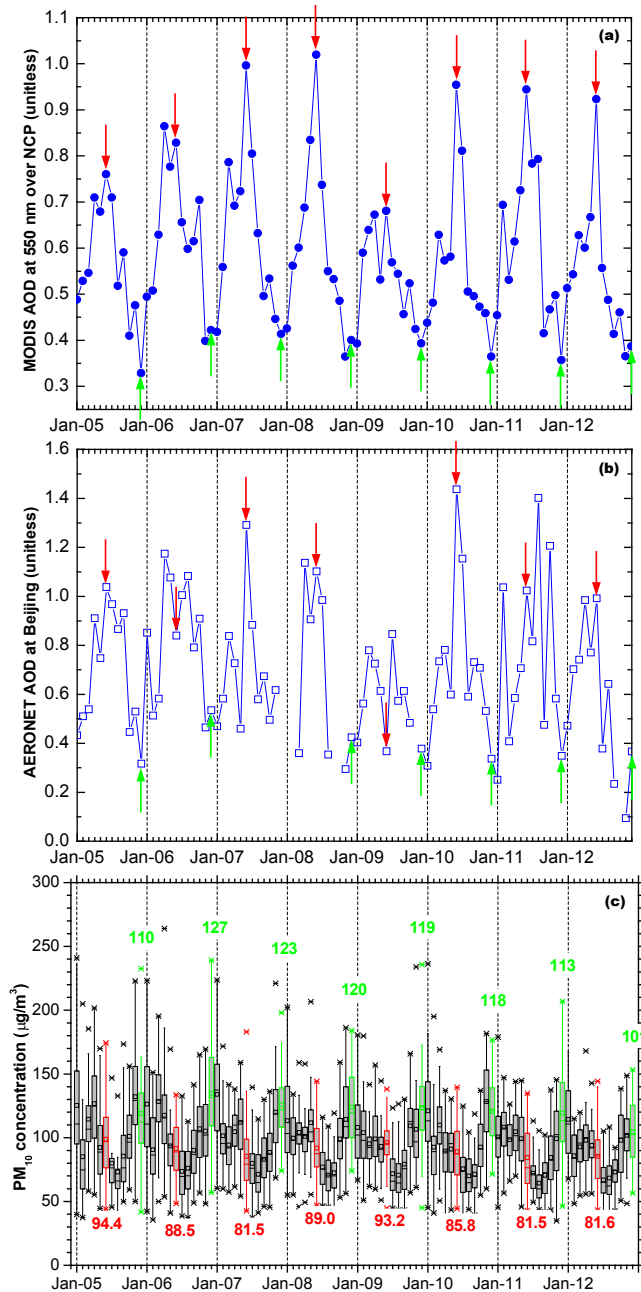


Fig. 2. (a) MODIS Terra monthly averaged AOD at 550 nm over NCP from January 2005 to December 2012. The red and green arrows indicate AOD in June and December, respectively. (b) AERONET monthly averaged AOD (interpolating using values at 440 nm and 675 nm) at Beijing (116.381° N, 39.977° E) from January 2005 to December 2012. The red and green arrows indicate AOD in June and December, respectively. (c) Monthly PM₁₀ mass concentration in 34 major Chinese cities over NCP from 2005 to 2012. The box-and-stem plots depict the minimum, the 1st, 5th, 25th, 50th (median), 75th, 95th, 99th percentile and the maximum for the PM₁₀ concentration; the square in the box depicts the arithmetic mean. The geometric mean of the monthly PM₁₀ concentration for the 34 cities in June and December also presented. Those in June and December are shown in red and green, respectively. (For interpretation of the references to colour in this figure legend, the reader is referred to the web version of this article.)

are much higher than those in December. The higher extinction coefficient above ~600 m in the vertical profile in June (compared with that in December) is consistent with the higher BLH (favorable for more efficient transport and mixing of particles to a higher altitude) as well as the higher column integrated AOD. The peak

extinction coefficient layers located aloft in the June profiles (relative to the December profiles) and the significant difference in extinction coefficient between higher altitude and near surface in Fig. 3b can interpret the higher AOD and lower surface PM concentration in June.

Fig. 3e shows the monthly average BLH over the area of 30–40° N and 110–120° E during 2000–2013. As BLH is much different between land and ocean (Fig. 3a), 120° E is chosen as the east boundary to plot the monthly BLH time series over the major land area within the study area. A comparably higher BLH is found in June (only slightly lower than that in May and April), consistent with the higher AOD then. On the contrary, a lower BLH in December (Fig. 3e) is consistent with the lowest AOD over NCP in December (Fig. 2a and b).

4.3. Other meteorological and topographical factors

NCP is an eastward open topographical basin surrounded by the Yanshan Mountains to the north, by the Taihang Mountains and the Qinling Mountains to the west, and by the Daba Mountains and the Dabie Mountains to the south (see supplementary material 1). The difference of wind vector between June and December illustrates a prevailing inshore (southeast and south) wind in June (Fig. 3c), which favors accumulation of the pollutants (originated from the intensive anthropogenic emission in this densely populated region) within the topographical basin of NCP and influx of the moisture from the ocean. Correspondingly, the RH profile (Fig. 3d) as well as the difference of RH between June and December at 850 hPa level (Fig. 3c) demonstrates a higher RH in June from 1000 hPa to 300 hPa levels over the AOD hotspots area of NCP. Meanwhile, a significant increase of RH from May to June is obvious at 1000 hPa, 925 hPa and 850 hPa levels over the area of 30–40° N and 110–120° E (Fig. 3f). Here the 850 hPa pressure level, which is comparable to ~1900 m of the average BLH in June (Fig. 3e), is chosen to reflect RH at the upper level of the boundary layer (BL). Such an increase of RH in June at different levels is favorable for enhancement in new particle speciation (NPS) and secondary aerosol formation (such as sulfate and organic aerosol, Sun et al., 2013) as well as in hygroscopic growth of the aerosol (Qu et al., 2015a); all these processes can subsequently result in enhanced aerosol extinction as well as increase of the column AOD and impairment of visibility (Vis).

Indeed, increase of AOD is found to be associated with increase of the total column water vapor content (CWV, Smirnov et al., 2002; Eck et al., 2008). Bi et al. (2014) identified a strong positive correlation between AOD and CWV at Beijing in January 2013. Aerosol water content was found to contribute significantly to the light extinction under Asian continental outflow (Jung and Kim, 2011), and its effect on light extinction and Vis impairment is mainly due to increases of the (NH₄)₂SO₄ and NH₄NO₃ concentration (Jung et al., 2009).

Along this line, a comparison of the GOCART (Mian et al., 2002) modeled CODs (column optical depth) of the aerosol components in 2000–2007 shows that sulfate has the greatest COD difference between June and December (supplementary material 3). The higher sulfate COD over NCP in June is consistent with the initial significant increase of RH from May to June (Fig. 3f), which confirms that increase of RH and enhancement of hygroscopic growth of sulfate (a major aerosol component) contribute crucially to the maximal AOD in June over NCP. Moreover, the high sulfate COD center (>0.1, shaded with blue to yellow) spans all over ECN in June but only limits within the more south part of ECN in December, consistent with the general spatial and temporal distribution of higher RH. Similarly, the high BC area also limits within the south part of ECN in December and shows a broadly northward extension in June, but with a weaker summer vs. winter contrast compared

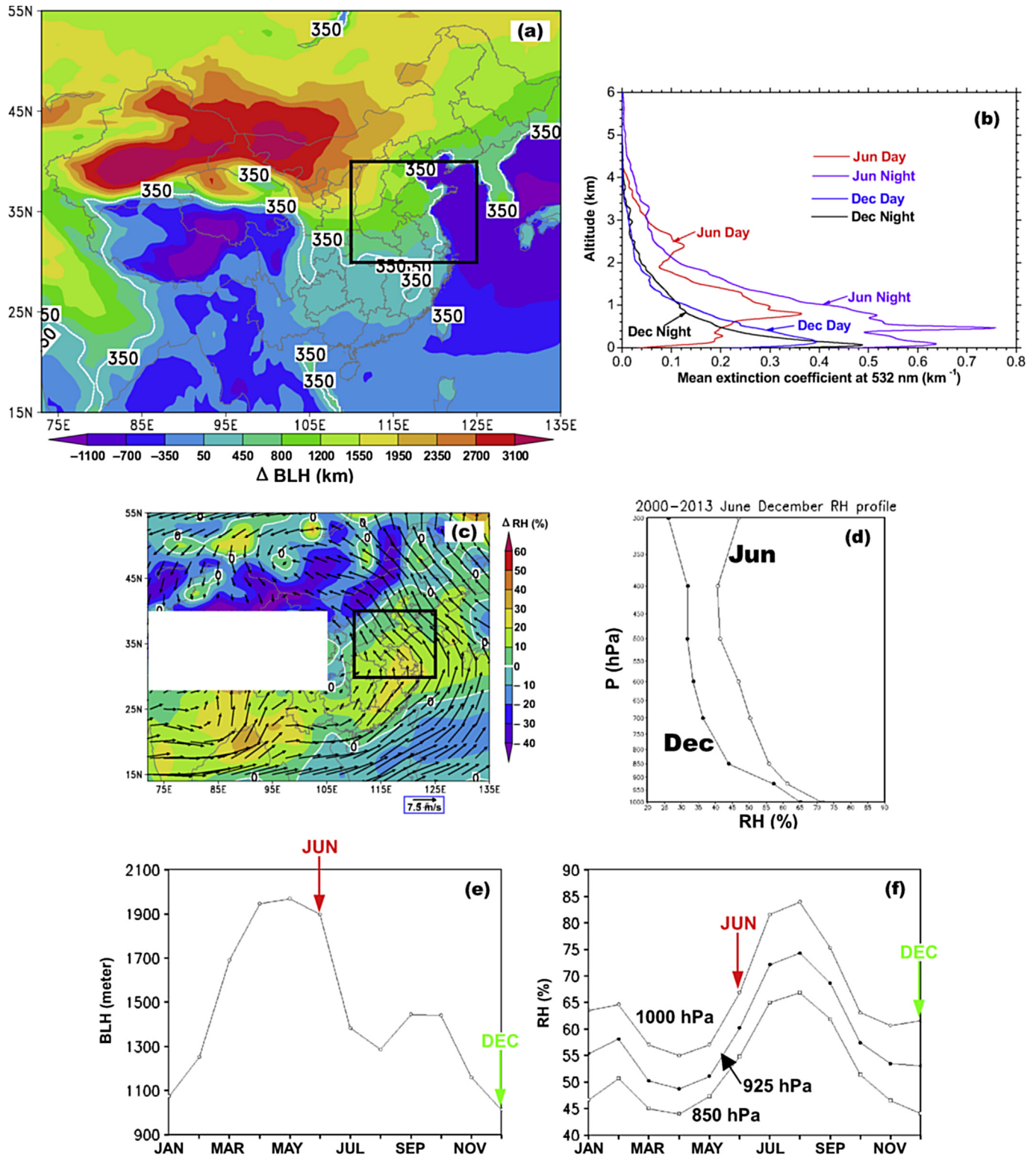


Fig. 3. (a) The difference of average boundary layer height (BLH, meter) at 14:00 local time between June and December ($\Delta BLH = BLH_{\text{June}} - BLH_{\text{December}}$) during 2000–2013. BLH in June is generally greater than BLH in December by at least 350 m over the AOD hotspots area from Shandong Peninsula to the north of Yangtze River in eastern China. The black box indicates NCP. (b) Vertical profile of the aerosol extinction coefficient at 532 nm (km^{-1}), derived from CALIPSO level 3 allsky product) over the area of 30–40° N and 110–120° E in June and December 2014. (c) The difference of mean wind vector and relative humidity (RH) between June and December (June minus December, $\Delta RH = RH_{\text{June}} - RH_{\text{December}}$) during 2000–2013 at 850 hPa (1475 gpm, geopotential height in meters) level, the white line illustrates the zero line of ΔRH (i.e., the mean RH in June is equal to that in December), the black box indicates NCP; the results at surface, 1000 hPa (110 gpm), 925 hPa (762 gpm) and 700 hPa (3012 gpm) levels are similar and not shown. The difference of RH generally shows a higher RH over the AOD hotspots area in June compared with December. (d) The RH profile in June and December over NCP during 2000–2013, a higher RH in June is obvious from 1000 hPa to 300 hPa levels. (e) The monthly average BLH over the area of 30–40° N and 110–120° E during 2000–2013. (f) Same as (e) but for relative humidity (RH, %) at 1000 hPa, 925 hPa and 850 hPa levels.

with sulfate (figures not shown). The June vs. December difference of CODs for other aerosol components is unobvious and not considered.

Furthermore, according to the IMPROVE (Interagency Monitoring of Protected Visual Environments) reconstruction method (<http://vista.cira.colostate.edu/improve/Tools/ReconBext/reconBext.htm>) for aerosol scattering (which is a major component of aerosol extinction), the scattering coefficient (B_{scat}) can be calculated using the following formula,

$$B_{\text{scat}} (\text{Mm}^{-1}) = 3f_T(\text{rh})[\text{Sulfate}] + 3f_T(\text{rh}) [\text{Nitrate}] + 4f_{\text{org}}(\text{rh}) [\text{OMC}] + 1 [\text{Soil}] + 0.6 [\text{CM}] \quad (1)$$

where [Sulfate] and [Nitrate] are mass concentrations calculated based on the forms of $(\text{NH}_4)_2\text{SO}_4$ and NH_4NO_3 , [OMC] is the organic mass by carbon, [Soil] is the mass of fine dust aerosol and [CM] is the coarse mass; while $f_T(\text{rh})$ and $f_{\text{org}}(\text{rh})$ are the relative humidity correction factors for converting dry scattering coefficient to ambient value. Three times of $f_T(\text{rh})$ and four times of $f_{\text{org}}(\text{rh})$ in formula (1) demonstrate that scattering of aerosol components such as sulfate, nitrate and organic matter can be strongly enhanced when RH increases, which supports the conjecture above that the higher RH and higher sulfate contribution to the aerosol profile over NCP in June are associated with an increase of AOD due to enhancement of the aerosol extinction efficiency.

In summary, the comparably higher BLH in June (Fig. 3e) is favorable for more efficient transport and mixing of particles to a higher elevation, which results in a higher AOD but a smaller surface PM concentration. On the contrary, in December the lower BLH (Fig. 3e) is associated with accumulation of the particles near surface but a lower extinction coefficient in the vertical profile (Fig. 3b) and subsequently a lower AOD. Moreover, accumulation of the pollutants within the eastward open topographical basin of NCP and influx of the moisture (as well as increase of RH) accompanied with the prevailing inshore wind in June (Fig. 3c) are also favorable for the enhancement of aerosol extinction and for the higher AOD over NCP. An integration of these factors is followed in section 5.

5. A simple model to reconcile AOD and PM seasonality

AOD is in proportion to the product of PM concentration, the shape of aerosol extinction profile (H) and RH correction factors ($f(\text{rh})$) (Kessner et al., 2013). Here the PM_{10} concentration during 2005–2012 and $\text{PM}_{2.5}$ concentration during 2014 in 34 major Chinese cities within NCP are used to calculate the monthly PM concentration. The monthly averaged BLH over NCP during 2005–2012 is used to reflect variation of H. RH at the 1000 hPa, 925 hPa and 850 hPa levels are used to calculate the monthly averaged RH within BL, which is subsequently used to determine $f(\text{rh})$ value (http://vista.cira.colostate.edu/improve/Tools/humidity_correction.htm). Note BLH at 14:00 local time is used, while RH and PM are derived from daily averages; these measurements are not coincident in time with the MODIS satellite overpass. Although monthly averages are compared here, disagreement is expected due to difference in the temporal coverage of measurements. Assuming the aerosol and water vapor are well mixed within BL, the PM concentration, $f(\text{rh})$ and BLH is used to establish a simple model, and $\text{PM}^*\text{BLH}^*f(\text{rh})$ can thus reflect the variation of AOD due to aerosol extinction in BL, which is subsequently compared with the monthly averaged MODIS AOD over NCP.

There is generally a synchronous variation between the monthly averaged monthly $\text{PM}^*\text{BLH}^*f(\text{rh})$ and AOD over NCP (with a June maximum and a December minimum, Fig. 4a and b); moreover, significant correlations also exist between $\text{PM}^*\text{BLH}^*f(\text{rh})$ and AOD ($R^2 = 0.81$ and 0.74 for PM_{10} and $\text{PM}_{2.5}$, respectively,

$P < 0.0005$, $n = 12$, Fig. 4d and e). Although individually PM, BLH and $f(\text{rh})$ can not well explain the AOD variation, BLH in collaboration with the surface PM concentration (PM) and the RH correction factor ($f(\text{rh})$) can explain about 81% or 74% of the variance of monthly averaged AOD over NCP. Consequently, the simple model supports our discussion in section 4 that the large values of BLH, RH and the corresponding emission and PM concentration are major possible causes of the maximal AOD in June over NCP. Note here only the available surface PM concentration is used in the comparison between $\text{PM}^*\text{BLH}^*f(\text{rh})$ and AOD.

Moreover, analysis on individual cities in the specific months identifies significant ($P < 0.0001$ significance level) correlation ($R^2 = 0.12$ – 0.41 , $n = 103$ – 151) between $\text{PM}_{10}^*\text{BLH}^*f(\text{rh})$ and AOD for 22 of the 34 cities over NCP (for more detail see [supplementary material 4](#)); the unmatched AOD, BLH and RH (extracted from 1.0, 0.125 and 2.5° grid data) and PM_{10} concentration (measured at a specific location) is an expected source of error, and averaging over space and time could result in better agreement between $\text{PM}_{10}^*\text{BLH}^*f(\text{rh})$ and AOD (discussed above). Indeed, the monthly area averaged $\text{PM}_{10}^*\text{BLH}^*f(\text{rh})$ and AOD over NCP during 2004–2012 varied synchronously (Fig. 4c), and a stronger correlation ($R^2 = 0.53$, $P < 0.0001$ significance, $n = 103$, Fig. 4f) is found between them.

6. Preliminary hypothesis about impact of EASM front

It is well known that the shift of the winter and summer monsoon is a major characteristic of weather and climate over East Asia. Climatologically, the phasic northward progress of the summer monsoon front (SMF) experiences three times abrupt advance and four quiescent stages each year. SMF is located at the north part of south China during its first quiescent stage (May 16 to June 10, SMF1, Fig. 5a), and then marches to the Yangtze River Basin, the Yellow River and Huai River Basin, and north China during its second (June 16 to July 5, SMF2), third (July 6 to July 20, SMF3) and fourth (July 21 to August 10, SMF4) quiescent stages, respectively (Wu, 2002). To facilitate the discussion, SMF0 (Apr 20 to May 15), a period with the same duration of but before SMF1, is defined to supply a background before the East Asia summer monsoon (EASM) developing.

Monthly variation shows an abrupt increase of AOD over NCP from May to June (Fig. 4a). More specifically, there is an obvious AOD increase over NCP from SMF0 (Fig. 6a) to SMF1 (Fig. 6b); meanwhile, the higher AOD (>0.9 , shaded with red) area over ECN experiences a further northward displacement from SMF1 (Fig. 6b) to SMF2 (Fig. 6c). Correspondingly, the PM_{10} concentration exhibits a comparably higher value from December to May (Fig. 2c, associated with additional emission from house heating in winter and contribution from dust in spring), followed by June with the highest PM_{10} concentration in summer (June, July and August). Similar variation for the one-year record of monthly $\text{PM}_{2.5}$ concentration in 2014 ([supplementary material 2](#)) also indicated the highest June PM concentration in summer. More in detail, the difference between SMF1 and SMF0 shows a significant increase of $\text{PM}_{2.5}$ concentration over the major south part of ECN (Fig. 7a), which is consistent with the increase of multi-year averaged RH from SMF0 to SMF1 in this region (Fig. 7c). A comparison of the spatial distribution of $\text{PM}_{2.5}$ and RH differences shows that the area with a slight and initial RH increase (0–2%, shaded with green in Fig. 7c) seems like the area with a greater $\text{PM}_{2.5}$ increase (generally $> 15 \mu\text{g m}^{-3}$, Fig. 7a). These AOD and PM variations could be interpreted by a preliminary hypothesis of the possibly enhanced formation of the secondary aerosol (SOA) accompanied with the northward progress of EASM (as conceptually illustrated in Fig. 5b).

The spatial displacement of SMF associated with EASM

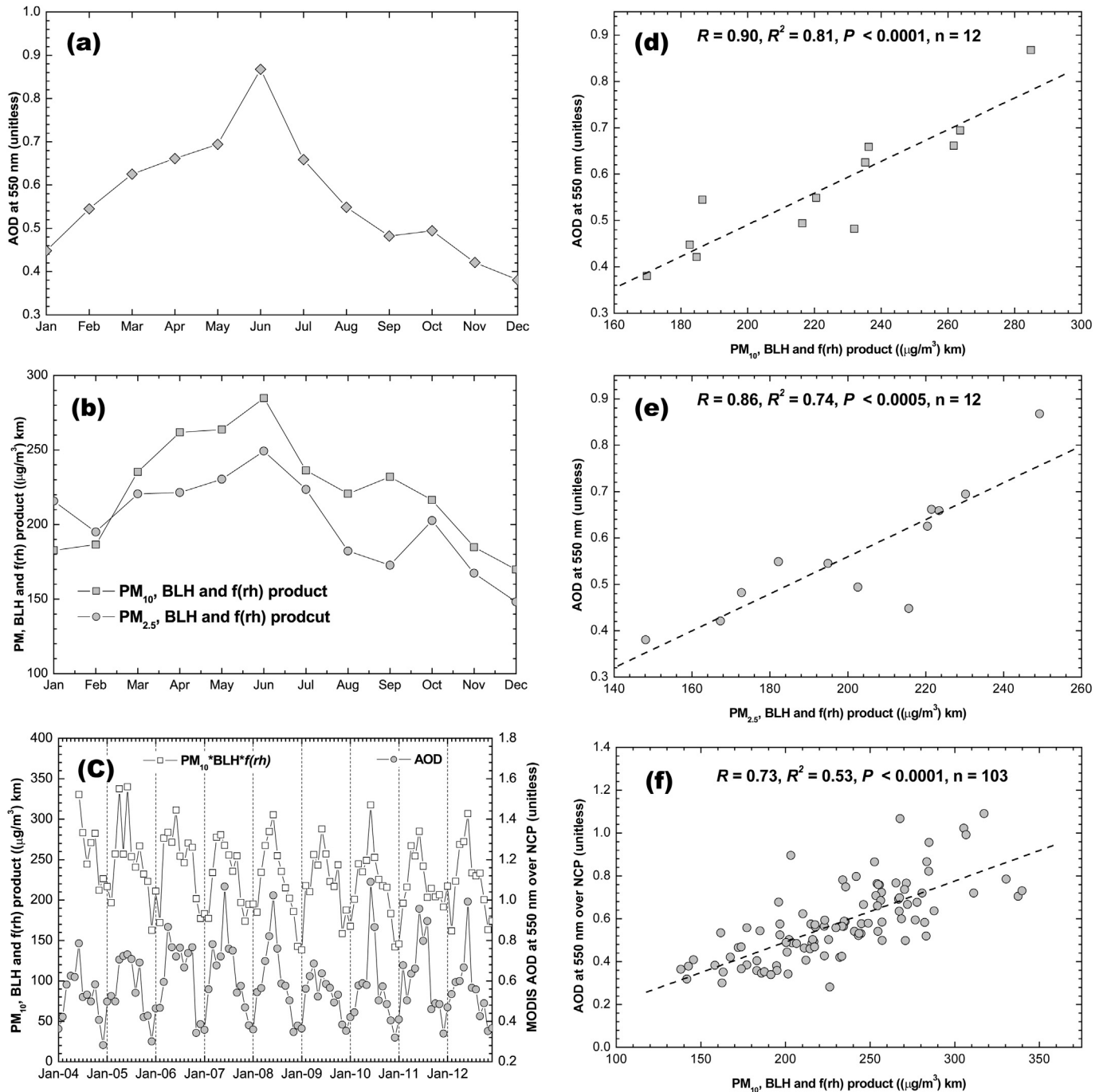


Fig. 4. (a) MODIS Terra monthly averaged AOD at 550 nm over NCP during 2001–2013. (b) Monthly product of PM concentration, boundary layer height (BLH, at 14:00 local time) and RH correction factors ($f(rh)$) ($\text{PM} \cdot \text{BLH} \cdot f(rh)$) over NCP. (c) Time series of the monthly area averaged $\text{PM}_{10} \cdot \text{BLH} \cdot f(rh)$ and AOD over NCP during 2004–2012. (d) Linear fitting between the monthly averaged AOD and $\text{PM}_{10} \cdot \text{BLH} \cdot f(rh)$ over NCP. (e) Same as (d) but for $\text{PM}_{2.5}$. (f) Same as (d) but for the monthly area averaged $\text{PM}_{10} \cdot \text{BLH} \cdot f(rh)$ and AOD over NCP during 2004–2012.

development can result in changes in the converging of precursor gases (of aerosol) with moisture introduced by EASM into the region. The key point here is that during the drier period before EASM prevailing (i.e., the winter and spring associated with presumably more intensive anthropogenic emission), although the aerosol precursor gases is abundant in the atmosphere, the water vapor is presumably in deficit over ECN and serves as an important rate control condition for SOA formation. In this context, northward introduction of the water vapor into ECN and increase of RH during

the early phase of EASM development is crucial to SOA formation. When converging and mixing of the precursor gases of aerosol with the moisture from south occur, ECN becomes a good place with more efficient photochemical activity, leading to enhancement of NPS, SOA formation and hygroscopic growth. Indeed, the NPS events in urban Beijing were usually associated with changes in wind directions (Zhang et al., 2011), implying that mixing of the precursor gases with moisture (occurred during converging of different air masses) is favorable for photochemical activities and

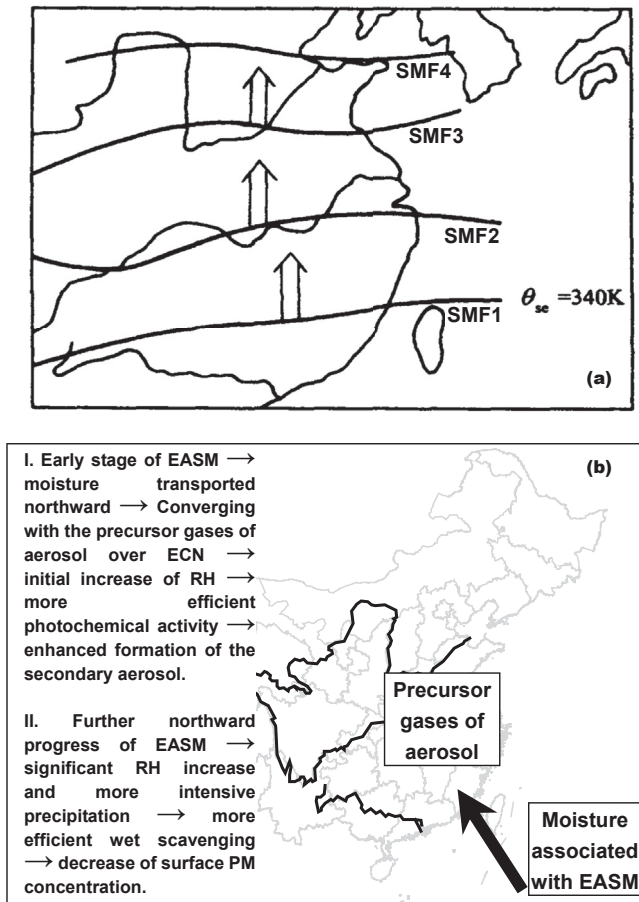


Fig. 5. (a) Change of the summer monsoon front (SMF) illustrated by the average position of the 850 hPa level pseudoequivalent potential temperature $\theta_{se} = 340$ K contour during 1971–1980 (follow Wu et al., 2002). Here SMF1, SMF2, SMF3 and SMF4 are corresponding to May 16 to June 10, June 16 to July 5, July 6 to July 20 and July 21 to August 10, respectively; the average positions of SMF during these four quiescent stages are demonstrated (detail in section 6 of the main text). (b) A conceptual illustration of the enhanced formation of the secondary aerosol due to northward transport of the moisture (as well as initial increase of relative humidity, RH) and subsequent converging and mixing with the precursor gases of aerosol over eastern China (ECN) during the early stage of the East Asia summer monsoon (EASM), which results in more efficient photochemical activity. Further northward progress of EASM is associated with increased precipitation and more efficient wet scavenging, which result in decrease of the surface particulate matter (PM) concentration.

NPS, which supports our hypothesis above. Such an enhanced SOA formation can potentially influence AOD and PM concentration. Here, $PM_{2.5}$ concentration is used to evaluate the PM variation associated with SOA formation because SOA should be within the size range of fine particle.

On the other hand, for the area of Guangdong Province (the most south of ECN, nearby Hainan Island) with a significant RH increase from SMF0 to SMF1 (2%–8%, shaded with yellow to orange in Fig. 7c), the $PM_{2.5}$ concentration decreases (Fig. 7a), probably due to more efficient wet scavenging when RH increases further. This is confirmed by the shift from SMF1 to SMF2, accompanying with a general significant increase of RH (>10%, Fig. 7d) and a decrease of $PM_{2.5}$ concentration (Fig. 7b) over the major area of ECN.

Moreover, variation of Vis accompanied with the northward progress of EASM also supports our hypothesis. As Vis shows an interannual decreasing trend over ECN (Qu et al., 2013, 2015b), here the normalized Vis is calculated based on each station during May 16 to August 10 (i.e., the period spans over the four quiescent stages of SMF) each year to assess the phasic variation of Vis due to the

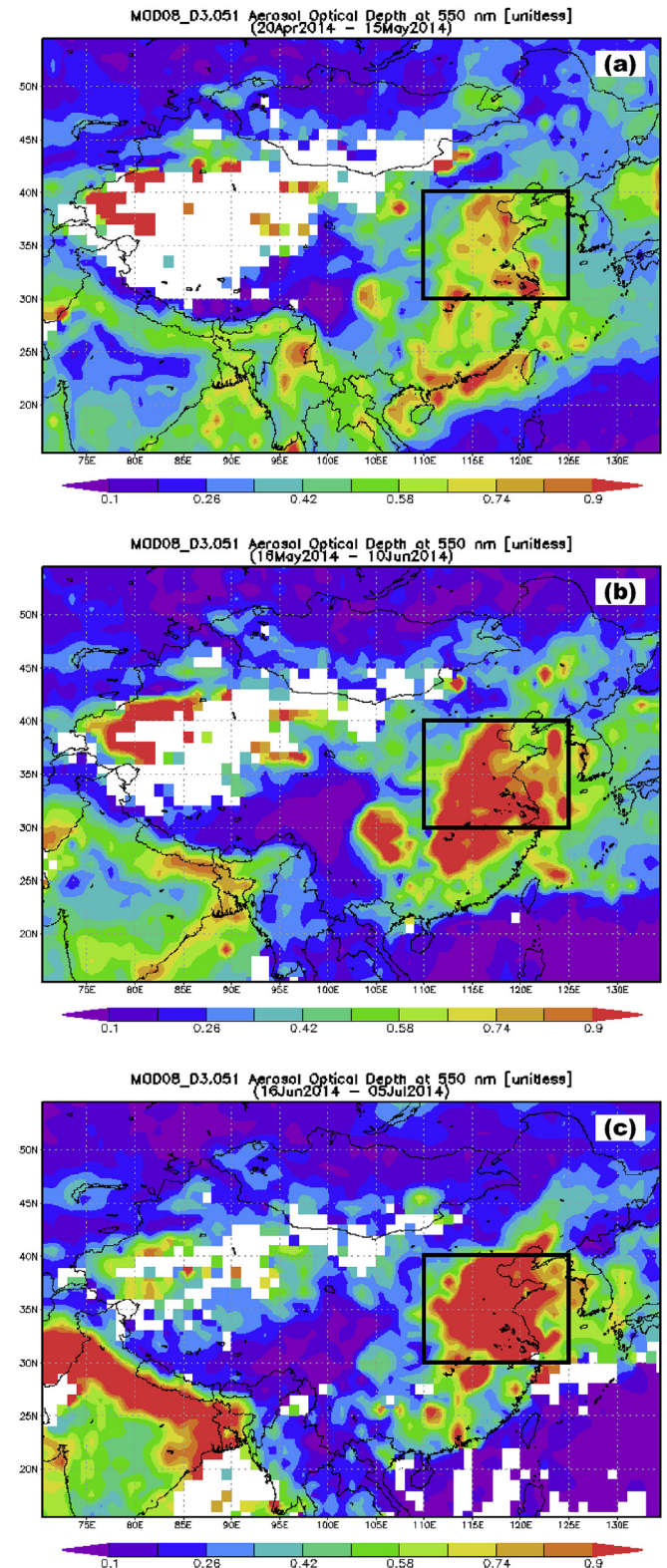


Fig. 6. The mean MODIS Terra AOD at 550 nm over China during (a) Apr 20 to May 15 (SMF0), (b) the first quiescent stage of the summer monsoon front (SMF1, May 16 to June 10), and (c) the second quiescent stage of the summer monsoon front (SMF2, June 16 to July 5) in 2014. The black box indicates NCP.

northward progress of SMF. Our analysis finds that the south part of ECN experiences a Vis improvement accompanied with the northward progress of SMF, while NCP (30–40° N and 110–125° E)

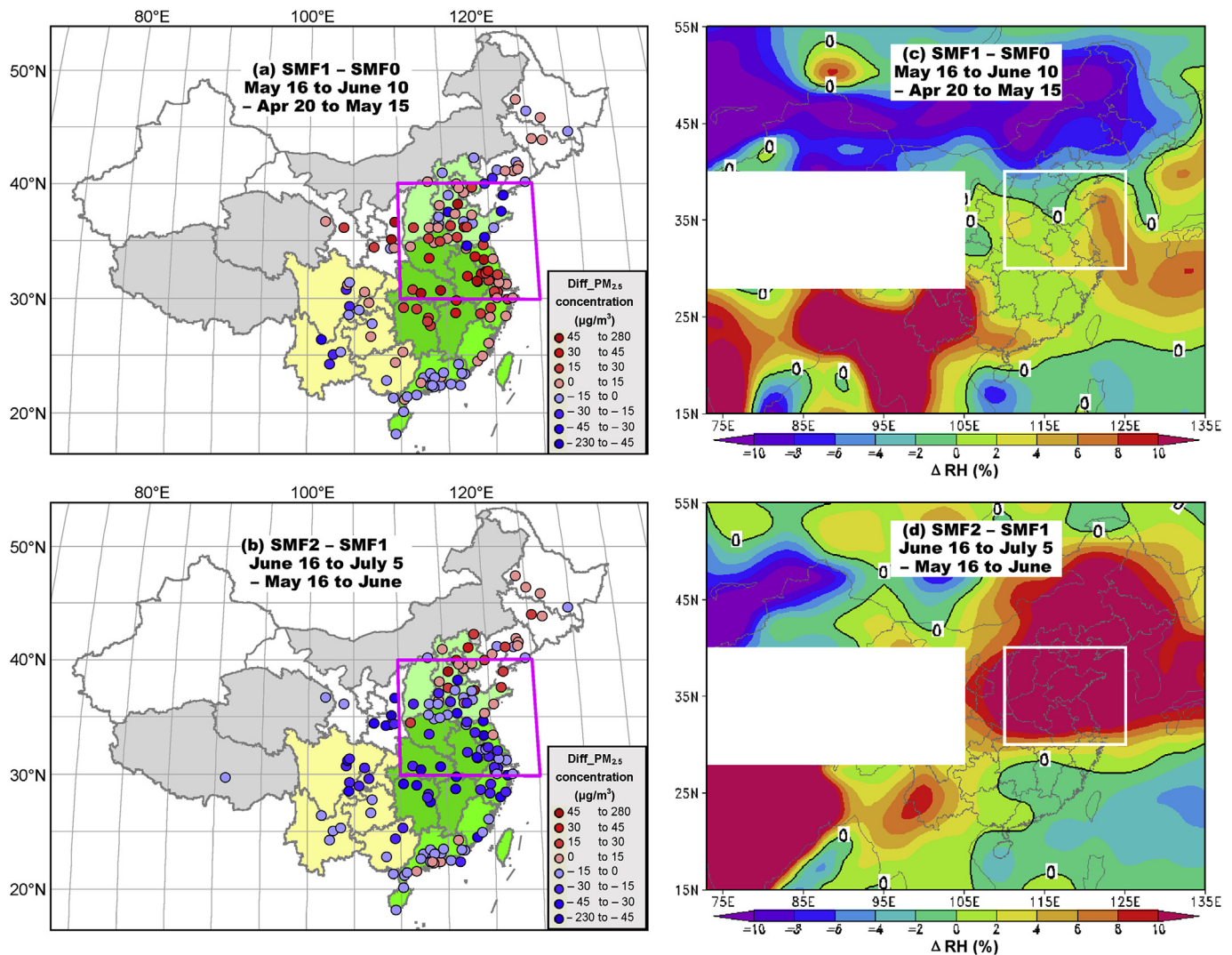


Fig. 7. Difference of the surface PM_{2.5} concentration (μg/m³) in 142 Chinese cities (a) between the first quiescent stage of the summer monsoon front (SMF1, May 16 to June 10) and Apr 20 to May 15 (SMF0); (b) between the second quiescent stage of the summer monsoon front (SMF2, June 16 to July 5) and SMF1. The magenta box indicates NCP. (c) and (d), same as (a) and (b) but for the difference of NCEP RH at 1000 hPa level during 2000–2013, black line illustrates the zero line of ΔRH, white box indicates NCP, values over topography higher than 1500 m (mostly the Tibetan Plateau) are masked out.

experiences a Vis degradation during the same course (supplementary material 5); the increase of RH and the decrease of surface wind speed (supplementary material 6, here wind speed is also normalized using the same method for Vis) might be possible causes favorable for enhancement of NPS and SOA formation as well as Vis degradation over NCP accompanied with the northward progress of SMF.

Based on these analyses, we can hypothesize the impact of EASM front on a possible enhancement of SOA formation, which contributes to the significant increase of PM_{2.5} concentration and the corresponding increase of AOD from SMF0 to SMF1 over NCP.

7. Conclusion

In contrast to the lower surface PM concentration in summer, AOD shows an obvious increase in summer (June) compared with winter (December) over NCP. Several factors work in concert to result in this opposite seasonality of AOD and surface PM.

- (i) Increase of BLH, associated with more efficient transport and mixing of particles to a higher altitude, results in a higher

extinction coefficient near and above the top of BLH and therefore, a higher AOD but a decrease of surface PM concentration over NCP in June.

- (ii) Converging and mixing of the precursor gases of aerosol with the moisture introduced by EASM, which subsequently results in an increase of RH and enhancement of NPS, SOA formation and hygroscopic growth (especially for sulfate as a major aerosol component).
- (iii) Emission from regional open stalk burning in the summer harvest season.
- (iv) The typical southeast and south wind and the mountains to the north and west (generally ≥ 1500 m above sea level) resulting in accumulation and restriction of pollutants within the NCP topographical “basin”.

BLH, RH in collaboration with PM concentration can well explain the multi-year averaged monthly variation of AOD. These factors need to be considered when investigating the climate effect of aerosol in the region.

The increase of AOD and PM concentration over NCP in early summer can be attributed to possible enhanced new particle

speciation and SOA formation during the early phase of EASM (section 6). The presumably intensive solar radiation, high RH and high temperature over ECN in summer are all favorable for the enhancement of photochemical activity and SOA formation. However, the suggested hypothesis should be further investigated. Observation and study on the contribution of SOA to the total aerosol, on the possibly seasonal variation of aerosol components, as well as on influx and impact of the ocean originated materials (such as sea salt, dimethylsulfide (Ma et al., 2005), etc.) accompanied with EASM should be helpful to improve our understanding in the future. Clarifying the variation of AOD and PM accompanied with the establishing and prevailing of EASM is potentially helpful to study the feedback and interaction between the increased aerosol loading and the variation of monsoon intensity in the region.

Acknowledgments:

This research is supported by NSFC 41276009 and Chinese Ministry of Education's 111 Project (B07036).

Appendix A. Supplementary data

Supplementary data related to this article can be found at <http://dx.doi.org/10.1016/j.atmosenv.2015.11.061>.

References

- Bi, J.R., Huang, J.P., Hu, Z.Y., Holben, B.N., Guo, Z.Q., 2014. Investigate the aerosol optical and radiative characteristics of heavy haze episodes in Beijing during January of 2013. *J. Geophys. Res.* <http://dx.doi.org/10.1002/2014JD021757>.
- Boynard, A., Clerbaux, C., Clarisse, L., Safieddine, S., Pommier, M., Damme, M.V., Bauduin, S., Oudot, C., Hadji-Lazaro, J., Hurtmans, D., Coheur, P.-F., 2014. First simultaneous space measurements of atmospheric pollutants in the boundary layer from IASI: a case study in the North China Plain. *Geophys. Res. Lett.* 41 <http://dx.doi.org/10.1002/2013GL058333>.
- Eck, T.F., Holben, B.N., Reid, J.S., Sinyuk, A., Dubovik, O., Smirnov, A., Giles, D., O'Neill, N.T., Tsay, S.-C., Ji, Q., Mandoos, A.A., Khan, M.R., Reid, E.A., Schafer, J.S., Sorokine, M., Newcomb, W., Slutsker, I., 2008. Spatial and temporal variability of column-integrated aerosol optical properties in the southern Arabian Gulf and United Arab Emirates in summer. *J. Geophys. Res.* 113, D01204. <http://dx.doi.org/10.1029/2007JD008944>.
- Engel-Cox, J.A., Holloman, C.H., Coutant, B.W., Hoff, R.M., 2004. Qualitative and quantitative evaluation of MODIS satellite sensor data for regional and urban scale air quality. *Atmos. Environ.* 38, 2495–2509.
- Hoff, R.M., Christopher, S.A., 2009. Remote sensing of particulate pollution from space: have we reached the promised land? *J. Air & Waste Manag. Assoc.* 59, 645–675.
- Jung, J., Lee, H., Kim, Y.J., Liu, X., Zhang, Y., Gu, J., Fan, S., 2009. Aerosol chemistry and the effect of aerosol water content on visibility impairment and radiative forcing in Guangzhou during the 2006 Pearl River Delta campaign. *J. Environ. Manag.* 90, 3231–3244.
- Jung, J., Kim, Y.J., 2011. Tracking sources of severe haze episodes and their physicochemical and hygroscopic properties under Asian continental outflow: long-range transport pollution, postharvest biomass burning, and Asian dust. *J. Geophys. Res.* 116, D02206. <http://dx.doi.org/10.1029/2010JD014555>.
- Kessner, A.L., Wang, J., Levy, R.C., Colarco, P.R., 2013. Remote sensing of surface visibility from space: a look at the United States East Coast. *Atmos. Environ.* 81, 136–147.
- Kong, W., Yi, F., 2015. Convective boundary layer evolution from lidar backscatter and its relationship with surface aerosol concentration at a location of a central China megacity. *J. Geophys. Res.* 120, 7928–7940.
- Li, C., Mao, J., Lau, K.A., Chen, J., Yuan, Z., Liu, X., Zhu, A., Liu, G., 2003. Characteristics of distribution and seasonal variation of aerosol optical depth in eastern China with MODIS products. *Chin. Sci. Bull.* 48, 2488–2495.
- Li, W.J., Shao, L.Y., Buseck, P.R., 2010. Haze types in Beijing and the influence of agricultural biomass burning. *Atmos. Chem. Phys.* 10, 8119–8130.
- Li, Z., Li, L., Zhang, F., Li, D., Xie, Y., Xu, H., 2015. Comparison of aerosol properties over Beijing and Kanpur: optical, physical properties and aerosol component composition retrieved from 12 years ground-based Sun-sky radiometer remote sensing data. *J. Geophys. Res.* 120, 1520–1535.
- Ma, Q., Hu, M., Zhu, T., Liu, L., Dai, M., 2005. Seawater, atmospheric dimethylsulfide and aerosol ions in the Pearl River Estuary and the adjacent northern South China Sea. *J. Sea Res.* 53, 131–145.
- Mian, C., Paul, G., Stefan, K., Omar, T., Brent, N.H., Bryan, N.D., Randall, V.M., Jennifer, A.L., Akiko, H., Teruyuki, N., 2002. Tropospheric aerosol optical thickness from the GOCART model and comparisons with satellite and sun photometer measurements. *J. Atmos. Sci.* 59, 461–483.
- Qu, W.J., Arimoto, R., Zhang, X.Y., Zhao, C.H., Wang, Y.Q., Sheng, L.F., Fu, G., 2010. Spatial distribution and interannual variation of surface PM₁₀ concentrations over eighty-six Chinese cities. *Atmos. Chem. Phys.* 10, 5641–5662.
- Qu, W., Wang, J., Gao, S., Wu, T., 2013. Effect of the strengthened western Pacific subtropical high on summer visibility decrease over eastern China since 1973. *J. Geophys. Res.* 118, 7142–7156.
- Qu, W.J., Wang, J., Zhang, X.Y., Wang, D., Sheng, L.F., 2015a. Influence of relative humidity on aerosol composition: impacts on light extinction and visibility impairment at two sites in coastal area of China. *Atmos. Res.* 153, 500–511.
- Qu, W., Wang, J., Zhang, X., Yang, Z., Gao, S., 2015b. Effect of cold wave on winter visibility over eastern China. *J. Geophys. Res.* 120 <http://dx.doi.org/10.1002/2014JD021958>.
- Smirnov, A., Holben, B.N., Dubovik, O., O'Neill, N.T., Eck, T.F., Westphal, D.L., Goroch, A.K., Pietras, C., Slutsker, I., 2002. Atmospheric aerosol optical properties in the Persian Gulf. *J. Atmos. Sci.* 59 (3), 620–634.
- Sun, Y.L., Wang, Z.F., Fu, P.Q., Jiang, Q., Yang, T., Li, J., Ge, X.L., 2013. The impact of relative humidity on aerosol composition and evolution processes during wintertime in Beijing, China. *Atmos. Environ.* 77, 927–934.
- Wang, J., Christopher, S.A., 2003. Intercomparison between satellite-derived aerosol optical thickness and PM_{2.5} mass: implications for air quality studies. *Geophys. Res. Lett.* 30 (21), 2095. <http://dx.doi.org/10.1029/2003GL018174>.
- Wang, K.C., Dickinson, R.E., Su, L., Trenberth, K.E., 2012. Contrasting trends of mass and optical properties of aerosols over the Northern Hemisphere from 1992 to 2011. *Atmos. Chem. Phys.* 12, 9387–9398.
- Wu, R.S., 2002. Principles of Modern Synoptic Meteorology. Higher Education Press, Beijing (in Chinese), 319pp.
- Xia, X.A., Chen, H.B., Wang, P.C., Zhang, W.X., Goloub, P., Chatenet, B., Eck, T.F., Holben, B.N., 2006. Variation of column-integrated aerosol properties in a Chinese urban region. *J. Geophys. Res.* 111, D05204.
- Yang, K., Dickerson, R.R., Carn, S.A., Ge, C., Wang, J., 2013a. First observations of SO₂ from the satellite Suomi NPP OMPS: widespread air pollution events over China. *Geophys. Res. Lett.* 40 <http://dx.doi.org/10.1002/grl.50952>.
- Yang, Y.J., Fu, Y.F., Wu, B.W., Shi, C.E., Deng, X.L., Zhang, H., Zhang, Y., 2013b. Impacts of agricultural fire on aerosol distribution over East China during summer harvest time. *J. Atmos. Environ. Opt.* 8 (4), 241–252.
- Zhang, Y.M., Zhang, X.Y., Sun, J.Y., Lin, W.L., Gong, S.L., Shen, X.J., Yang, S., 2011. Characterization of new particle and secondary aerosol formation during summertime in Beijing, China. *Tellus* 63B, 382–394.
- Zhao, X.J., Zhao, P.S., Xu, J., Meng, W., Pu, W.W., Dong, F., He, D., Shi, Q.F., 2013. Analysis of a winter regional haze event and its formation mechanism in the North China Plain. *Atmos. Chem. Phys.* 13, 5685–5696.